Diffusion of HDO into Single-Crystal $H_2{}^{16}O$ Ice Multilayers: Comparison with $H_2{}^{18}O$

F. E. Livingston, G. C. Whipple, and S. M. George*

Department of Chemistry and Biochemistry, University of Colorado, Boulder, Colorado 80309-0215

Received: October 11, 1996; In Final Form: January 22, 1997[⊗]

The diffusion of HDO into ultrathin single-crystal $H_2{}^{16}O$ ice multilayers was investigated using a novel combination of laser-induced thermal desorption (LITD) probing and isothermal desorption depth-profiling. The single-crystal hexagonal ice multilayers were grown epitaxially on a Ru(001) metal substrate, and the diffusion coefficients were measured perpendicular to the basal (0001) facet. The measured HDO diffusion coefficients ranged from $D = (2.2 \pm 0.3) \times 10^{-16}$ to $D = (3.9 \pm 0.4) \times 10^{-14}$ cm^2/s over the temperature range 153−170 K. Arrhenius analysis of the temperature-dependent diffusion coefficients yielded a diffusion activation energy of $E_A = 17.0 \pm 1.0$ kcal/mol and a preexponential factor of $D_0 = (4.2 \pm 0.8) \times 10^8$ cm^2/s. The similarity of the diffusion coefficients for HDO and $H_2{}^{18}O$ indicates that H/D exchange does not contribute significantly to HDO diffusion in ice. The agreement between the diffusion kinetics for HDO and $H_2{}^{18}O$ argues that the HDO diffusion occurs via a molecular transport mechanism. The large diffusion preexponentials for both HDO and $H_2{}^{18}O$ diffusion into the ultrathin ice multilayers also suggest that bulk transport properties in ice may be perturbed by close proximity to the ice surface.

I. Introduction

Chemical and physical processes occurring at the surface and in the bulk of crystalline ice have received significant attention. Surface and bulk diffusion phenomena in ice are important in such diverse fields as biology,[1−3] nuclear radiation chemistry,[4] and atmospheric and environmental chemistry.[5−9] In particular, heterogeneous atmospheric reactions on polar stratospheric cloud (PSC) particles composed of water−ice (type II PSC) and nitric acid−ice hydrates (type I PSC) are known to play a critical role in the seasonal depletion of Antarctic ozone.[5−8] Diffusion processes in ice are also related to relaxation and transport properties including mechanical[1] and dielectric[1,10−12] relaxation, electrical conductivity,[1] and defect formation and migration.[1,13−15]

The bulk diffusion of H_2O in crystalline ice has been explored previously by many researchers.[16−22] These early studies primarily used microtome and scintillation tracer techniques to measure the self-diffusion coefficients of $H_2{}^{18}O$, D_2O, and T_2O. Because the H_2O self-diffusion coefficients in ice are small, these isotopic tracer diffusion studies were performed at relatively high temperatures of $T = 238-273$ K close to the ice melting point. The measured H_2O diffusion coefficients were very similar for all the isotopic probe molecules with a typical value of $D \sim 2 \times 10^{-11}$ cm^2/s at $T = 263$ K.[1] Activation energies for H_2O self-diffusion have ranged from $E_A = 12.4$ to $E_A = 15.7$ kcal/mol, and the corresponding preexponential factors have varied from $D_0 = 0.6$ to $D_0 = 330$ cm^2/s.

In addition to the isotopic tracer experiments, *in situ* X-ray topography[13,15] has also been used to measure the growth of dislocation loops and dipoles on the surface of crystalline H_2O−ice originating from interstitial molecules. These X-ray measurements indirectly yielded H_2O self-diffusion coefficients ranging from $D = 1.8 \times 10^{-13}$ to $D = 6.8 \times 10^{-12}$ cm^2/s for $T = 221-252$ K. The H_2O diffusion activation energy of $E_A = 12.9$ kcal/mol and preexponential factor of $D_0 = 1.21$ cm^2/s derived from the X-ray topographic studies are also in very good agreement with the values previously obtained from isotopic tracer experiments. The correlation between the isotopic tracer and X-ray topographical measurements argues strongly for an interstitial diffusion mechanism.

Laser-induced thermal desorption (LITD) techniques have been utilized recently to study $H_2{}^{18}O$ diffusion into ultrathin single-crystal $H_2{}^{16}O$ ice multilayers.[23] Rapid $H_2{}^{18}O$ diffusion was observed into the crystalline ice bulk. The measured diffusion coefficients ranged from $D = (3.0 \pm 0.6) \times 10^{-16}$ to $D = (8.0 \pm 0.5) \times 10^{-15}$ cm^2/s for temperatures from $T = 155$ to 165 K. Arrhenius analysis of the diffusion constants over this temperature range yielded an activation energy of $E_A = 16.7 \pm 1.6$ kcal/mol and a preexponential factor of $D_0 = (9.7 \pm 0.5) \times 10^7$ cm^2/s. The diffusion activation energy determined using LITD techniques was within experimental error of some of the previous tracer measurements at higher temperatures near the ice melting point.[1]

The present study investigated the diffusion of HDO into single-crystal $H_2{}^{16}O$ ice multilayers grown epitaxially on Ru(001) and compared these results with the recent results for $H_2{}^{18}O$ diffusion. These experiments were performed at temperatures from $T = 153$ to 170 K that are significantly lower than the earlier isotopic tracer measurements. These temperatures are also closer to the temperatures in the polar stratosphere from 180 to 210 K. The diffusion of HDO was monitored in real time parallel to the *c*-crystal axis in hexagonal ice. The HDO and $H_2{}^{18}O$ diffusion coefficients and activation energies were compared and utilized to evaluate the mechanism of HDO diffusion into crystalline ice.

II. Experimental Section

A. Laser-Induced Thermal Desorption (LITD) Experimental Apparatus. The LITD experimental apparatus employed in the diffusion investigations has been described in detail elsewhere.[24,25] Briefly, the LITD measurements were conducted in an ultrahigh vacuum (UHV) chamber pumped by ion and titanium sublimation pumps that maintained typical background pressures $< 2 \times 10^{-10}$ Torr. A single-crystal Ru(001) substrate was used to grow epitaxial crystalline ice multilayers. Standard cleaning procedures were used to remove trace elemental (C, S, and O) contaminants from the Ru(001) crystal surface.[26] Confirmation of the ice film surface order and surface cleanliness of the Ru(001) substrate was accomplished using low-energy electron diffraction (LEED) and Auger electron spec-

[⊗] Abstract published in *Advance ACS Abstracts,* June 15, 1997.

S1089-5647(96)03252-X CCC: $14.00

troscopy (AES) with a single-pass cylindrical mirror analyzer (CMA).

The diffusion experiments were conducted using a novel combination of isothermal desorption depth-profiling and laser-induced thermal desorption probing.[23] A TEM-00 Q-switched Nd:phosphate glass laser was employed with an output wavelength of $\lambda = 1.06$ μm and pulse lengths of approximately 100 ns. Laser pulses with energies of ~0.20 mJ/pulse were focused onto the Ru(001) substrate at an incident angle of 54° with respect to the surface normal. This optical arrangement produces elliptical desorption areas with typical dimensions of ~150 μm × ~240 μm as measured by spatial autocorrelation methods.[27]

The crystalline ice film is transparent to the $\lambda = 1.06$ μm infrared radiation. However, the incident laser energy is absorbed efficiently by the underlying Ru(001) metal substrate. The irradiated surface area experiences a rapid localized temperature transient and thermally desorbs the H_2O molecules in the column region above the focused laser beam. The desorbed species are mass analyzed with high sensitivity using an Extrel C50 quadrupole mass spectrometer with line-of-sight to the ionizer.

B. Growth of Model Crystalline H_2O Ice Films. The structural properties of naturally occurring hexagonal ice (I_h) have been studied extensively by various scattering techniques[2] including X-ray, electron, and neutron diffraction. The I_h ice lattice is composed of a series of puckered layers, each of which consists of hexagonal rings of hydrogen-bonded water molecules. This molecular arrangement gives rise to an open lattice structure with a large intermolecular cohesion energy. Vacant shafts run both parallel and perpendicular to the *c*-crystal axis and result in the formation of the basal (0001) and prism ($10\bar{1}0$) facets, respectively.

Type II (water−ice) PSCs are believed to be crystalline and retain the hexagonal symmetry of I_h ice.[1,2,28,29] To investigate H_2O self-diffusion processes in ice that closely resemble stratospheric ice particles, crystalline H_2O ice multilayers were grown epitaxially on a single-crystal Ru(001) substrate. The single-crystal Ru(001) metal substrate has the closest lattice match of any single-crystal metal to the geometry of naturally occurring hexagonal ice. The lattice constant of the $(\sqrt{3} \times \sqrt{3})R30°$ unit cell on Ru(001) is 4.68 Å,[30] which closely matches the nearest-neighbor oxygen−oxygen distance of 4.50 Å in the first bilayer of the basal plane of I_h ice.[31]

A glass multichannel capillary array doser was used to adsorb gaseous H_2O (HPLC Grade, Fisher Scientific) onto the single-crystal Ru(001) surface. The crystalline ice multilayers were grown either by directed capillary H_2O vapor deposition at 160 K or by dosing the H_2O at 120 K followed by multilayer annealing at 160 K. Previous LEED measurements have confirmed that both methods of ice multilayer preparation yield highly ordered crystalline H_2O ice films.[23]

C. Measurement of HDO Diffusion by LITD−Desorption Depth Profiling. Measurements of HDO diffusion into single-crystal $H_2{}^{16}O$ ice films were performed by monitoring the HDO and $H_2{}^{16}O$ coverages in real time during isothermal multilayer desorption. A crystalline $H_2{}^{16}O$ ice multilayer was initially grown epitaxially on a Ru(001) substrate. The $H_2{}^{16}O$ ice multilayer was then exposed to deuterium oxide (D_2O, ≥99.996%, Cambridge Isotope Laboratories) at 120 K using a directed capillary array doser. Rapid isotopic H/D exchange at the ice multilayer surface resulted in the formation of a localized HDO adlayer as depicted pictorially in Figure 1a.

The HDO and $H_2{}^{16}O$ coverages were measured as a function of time by LITD probing during isothermal multilayer desorption. Initially, the HDO molecules are confined to the surface region by maintaining the Ru(001) crystal at very low temperatures ($T < 90$ K) using a liquid nitrogen-cooled cryostat in thermal contact with the Ru(001) surface. During isothermal multilayer desorption of the crystalline ice film, the HDO adlayer molecules can either diffuse into the underlying $H_2{}^{16}O$ ice bulk or desorb into the gas phase. Isothermal desorption of HDO molecules into vacuum will result in a concomitant decrease in the HDO number density in the ice multilayer and the HDO LITD signal.

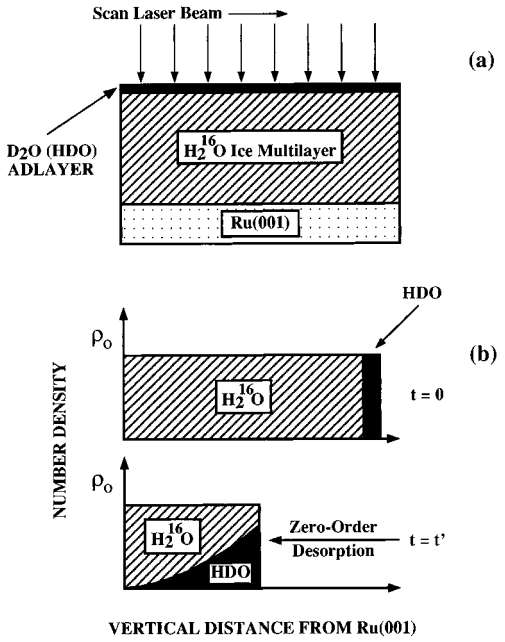

Figure 1. Schematic representation of the laser-induced thermal desorption (LITD) experiment. (a) Initial condition with the HDO isotope localized at the surface of the $H_2{}^{16}O$ ice multilayer. The laser beam is translated across the ice multilayer surface to measure the HDO and $H_2{}^{16}O$ coverages versus time. (b) HDO number density versus vertical distance from the Ru(001) surface at initial time $t = 0$ and after HDO diffusion and isothermal desorption depth-profiling at time $t = t'$.

Optical interference techniques have revealed previously that H_2O desorption from ice is independent of H_2O coverage and follows zero-order kinetics.[25,32] Zero-order isothermal desorption will reduce the ice multilayer thickness in a layer-by-layer fashion. Consequently, the isothermal desorption of H_2O from ice allows for depth profiling of the ice film as depicted in Figure 1b. During the isothermal desorption, the laser beam from the Nd:phosphate glass laser was translated across the ice multilayer using mirrors mounted on piezoelectric translators equipped with optical encoders. The HDO and $H_2{}^{16}O$ coverages were monitored until the ice multilayer was completely removed by isothermal desorption.

LITD was also used to measure the desorption kinetics of $H_2{}^{16}O$ ice multilayers. Briefly, a crystalline $H_2{}^{16}O$ ice multilayer was initially prepared, and then the $H_2{}^{16}O$ coverage was monitored versus time during isothermal desorption. The $H_2{}^{16}O$ desorption kinetics were measured over a wide temperature range ($T = 150-175$ K) to extract the desorption kinetic parameters. The activation energy for H_2O zero-order desorption from single-crystal ice grown epitaxially on Ru(001) was determined to be $E_d = 12.4 \pm 0.6$ kcal/mol, and the preexponential was $\nu_0 = (1.0 \pm 0.4) \times 10^{31}$ molecules/(cm^2 s). These H_2O desorption parameters are consistent with previous results derived from optical interference[25,32] and molecular beam experiments.[25]

D. Modeling of Simultaneous Diffusion and Desorption. Diffusion coefficients for HDO migration into single-crystal $H_2{}^{16}O$ ice multilayers were extracted through computer modeling of the competition between diffusion and isothermal desorption. To simulate the simultaneity of the diffusion and desorption processes, each bilayer was subdivided into a large number of sublayers. HDO is initially confined to the surface adlayer region, and the concentration of HDO at time $t = 0$ and position $(x - y) = 0$ can be defined as $\Theta_{HDO}(x)$. Each sublayer is then treated as an independent line source and is allowed to diffuse throughout the ice multilayer according to the relevant diffusion equation for a one-dimensional, instantaneous extended line source in an infinite medium[33]

$$\Theta_{HDO}(y,t) = \frac{1}{2}\Theta_{HDO}(x)\left\{\mathrm{erf}\left[\frac{h-(y-x)}{2\sqrt{D\Delta t}}\right] + \mathrm{erf}\left[\frac{h+(y-x)}{2\sqrt{D\Delta t}}\right]\right\} \quad (1)$$

where D is the diffusion constant, h is the width of each sublayer, $(y - x)$ is the diffusion distance, and Δt is the time required for one sublayer to desorb.

$\Theta_{HDO}(y,t)$ is the amount of HDO that diffuses into sublayer "y" from sublayer "x" after a time step Δt. Each diffusion/desorption time step Δt is defined by the zero-order kinetics of the $H_2{}^{16}O$ ice multilayer and involves two elementary steps. First, all sublayers are allowed to diffuse, generating a new concentration profile throughout the ice multilayer. Next, the top sublayer is desorbed, and HDO and $H_2{}^{16}O$ concentrations are appropriately updated in the various 1D-array elements. This two-step iterative process is repeated until all $H_2{}^{16}O$ sublayers have been isothermally desorbed. Typical diffusion simulations utilized ~2500 independent line sources and a time step of ~1 s.

Fick's second law for diffusion is a differential description of mass transfer that assumes spatial and temporal continuums and derivatives defined in the limit that $dt \rightarrow 0$ and $d(y - x) \rightarrow 0$. Consequently, the number of independent line sources utilized in the computer modeling studies (~2500 line sources) can be much larger than the number of H_2O bilayers present in a typical diffusion experiment (~100 BL of H_2O). A large number of independent line sources effectively simulate the continuous nature of the one-dimensional diffusion process. The number of line sources was varied between 10^2 and 10^4 with no measurable effect (<3%) on the extracted diffusion coefficients.

III. Results

A. HDO Diffusion into Single-Crystal $H_2{}^{16}O$ Ice Multilayers. Typical results for the normalized HDO and $H_2{}^{16}O$ LITD signals as a function of time during the isothermal depth-profiling are shown in Figure 2. The 96 BL $H_2{}^{16}O$ ice multilayer (1 BL = 1.06×10^{15} molecules/cm^2) was grown by directed capillary array dosing at 120 K followed by annealing at 160 K.

Approximately 1.5 BL of D_2O was then deposited onto the crystalline $H_2{}^{16}O$ ice multilayer at 120 K. Rapid and complete isotopic H/D exchange at the ice surface resulted in the formation of a localized 3 BL HDO adlayer. The HDO and $H_2{}^{16}O$ coverages were then monitored versus time using LITD probing and isothermal desorption depth-profiling at $T = 155.8$ K.

The rate of decrease in the $H_2{}^{16}O$ LITD signal versus time follows zero-order desorption kinetics, and the 96 BL $H_2{}^{16}O$ multilayer is completely desorbed after ~2400 s. Based on H_2O zero-order desorption kinetics, the 3 BL HDO adlayer should desorb from the crystalline ice surface in ~85 s if the HDO remained localized at the ice surface with no HDO/$H_2{}^{16}O$ interlayer mixing. The normalized HDO LITD signals, however, clearly reveal that HDO has diffused into the underlying crystalline ice multilayer, and HDO is detected throughout the desorption of the entire ice film. The solid line represents an optimum fit generated from the computer simulations of the diffusion experiment. This best fit corresponds to a HDO diffusion coefficient of $D = (7.2 \pm 0.2) \times 10^{-16}$ cm^2/s at $T = 155.8$ K. Error limits for the diffusion constant are denoted by the dashed lines in Figure 2.

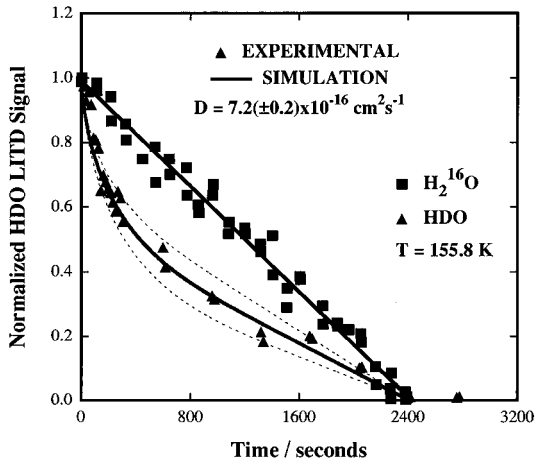

Figure 2. Diffusion experiment for 3 BL of HDO on 96 BL of $H_2{}^{16}O$ on Ru(001) at $T = 155.8$ K. The HDO and $H_2{}^{16}O$ LITD signals versus time are represented by solid triangles and squares, respectively. The solid line corresponding to the solid triangles represents a computer simulated best fit to the diffusion profile with $D(HDO) = (7.2 \pm 0.2) \times 10^{-16}$ cm^2/s. The error limits of the diffusion simulation are shown as dashed lines. The solid line associated with the solid squares represents a least-squares linear regression of the $H_2{}^{16}O$ isothermal desorption data.

The diffusion of HDO into single-crystal $H_2{}^{16}O$ ice multilayers was determined to be independent of H_2O film thickness and initial HDO number density. The diffusion coefficients measured at $T = 155.8$ K for $H_2{}^{16}O$ thicknesses of 48−123 BL and initial HDO adlayer thicknesses of 2−9 BL ranged from $D = 7.0 \times 10^{-16}$ to $D = 7.4 \times 10^{-16}$ cm^2/s.

B. Arrhenius Analysis of HDO Diffusion. The temperature dependence of the HDO diffusion coefficients was investigated to extract the kinetic parameters for HDO diffusion into crystalline $H_2{}^{16}O$ ice multilayers. The HDO diffusion constants varied from $D = (2.2 \pm 0.3) \times 10^{-16}$ to $D = (3.9 \pm 0.4) \times 10^{-14}$ cm^2/s over the temperature range $T = 153-170$ K. An Arrhenius plot of the measured HDO diffusion coefficients (solid triangles) for $T = 153-170$ K is shown in Figure 3. For comparison, the previously measured diffusion coefficients[23] corresponding to $H_2{}^{18}O$ migration into single-crystal $H_2{}^{16}O$ ice films at 155, 160, and 165 K are displayed as solid circles in Figure 3.

Arrhenius analysis of the HDO and $H_2{}^{18}O$ diffusion coefficients yielded the diffusion activation energies and preexponentials. For HDO, the kinetic parameters were $E_A(HDO) = 17.0 \pm 1.0$ kcal/mol and $D_0(HDO) = (4.2 \pm 0.8) \times 10^8$ cm^2/s. For $H_2{}^{18}O$, the kinetic parameters were $E_A(H_2{}^{18}O) = 16.7 \pm 1.6$ kcal/mol and $D_0(H_2{}^{18}O) = (9.7 \pm 0.5) \times 10^7$ cm^2/s. The error limits were derived from a weighted least-squares linear regression analysis of the Arrhenius diffusion data.

IV. Discussion

The present study investigated the diffusion of HDO into ultrathin single-crystal $H_2{}^{16}O$ ice multilayers grown epitaxially

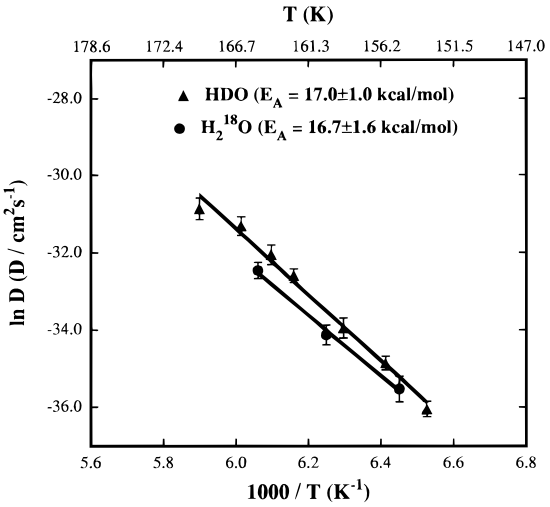

Figure 3. Comparison of the Arrhenius plots for the diffusion of HDO and $H_2{}^{18}O$ into single-crystal $H_2{}^{16}O$ ice multilayers on Ru(001). The kinetic parameters are $E_A(HDO) = 17.0 \pm 1.0$ kcal/mol, $D_0(HDO) = (4.2 \pm 0.8) \times 10^8$ cm^2/s, $E_A(H_2{}^{18}O) = 16.7 \pm 1.6$ kcal/mol, and $D_0(H_2{}^{18}O) = (9.7 \pm 0.5) \times 10^7$ cm^2/s. The error limits were derived from a weighted least-squares linear regression analysis.

on Ru(001). Measurements on ultrathin ice films provide several distinct advantages compared with macroscopic crystalline and polycrystalline ice. In particular, the use of LITD techniques on ultrathin H_2O films facilitates diffusion measurements on well-defined crystalline ice multilayers at low temperatures and short diffusion times. Typical diffusion measurements can be performed in real time with diffusion lengths of 10−400 Å and total diffusion times of 10^2-10^4 s. In contrast, the microtome and scintillation isotopic tracer experiments in macroscopic ice crystals require significantly longer time intervals of several days to weeks to observe diffusion lengths of >25 μm.

Because the crystalline ice is grown epitaxially on a single-crystal Ru(001) substrate, the H_2O−ice multilayers are highly ordered with low defect and dislocation densities. The close lattice match of the single-crystal Ru(001) metal to the geometry of hexagonal ice results in the growth of crystalline ice films with less than a 4% distortion compared with the ice I_h lattice.[30,31] In contrast, the early diffusion measurements on macroscopic ice samples[16−22] using isotopic tracer and microtome techniques are complicated by possible experimental artifacts such as surface diffusion, small angle defects, grain boundaries, and fluid inclusions.

The measured HDO diffusion coefficients ranged from $D(HDO) = (2.2 \pm 0.3) \times 10^{-16}$ to $(3.9 \pm 0.4) \times 10^{-14}$ cm^2/s for $T = 153-170$ K. A diffusion activation energy of $E_A(HDO) = 17.0 \pm 1.0$ kcal/mol and a preexponential factor of $D_0(HDO) = (4.2 \pm 0.8) \times 10^8$ cm^2/s were extracted from an Arrhenius analysis of the diffusion data. In comparison, the diffusion coefficients determined previously[23] for $H_2{}^{18}O$ migration into single-crystal $H_2{}^{16}O$ ice were $D(H_2{}^{18}O) = (3.0 \pm 0.6) \times 10^{-16}$ to $(8.0 \pm 0.5) \times 10^{-15}$ cm^2/s for $T = 155-165$ K. The kinetic parameters calculated for $H_2{}^{18}O$ diffusion were $E_A(H_2{}^{18}O) = 16.7 \pm 1.6$ kcal/mol and $D_0(H_2{}^{18}O) = (9.7 \pm 0.5) \times 10^7$ cm^2/s.

The similarity of the diffusion coefficients for HDO and $H_2{}^{18}O$ indicates that isotopic H/D exchange does not contribute significantly to HDO diffusion in crystalline ice. The close agreement between the diffusion kinetics for HDO and $H_2{}^{18}O$ also argues that HDO diffusion occurs primarily via a molecular transport mechanism. Molecular HDO migration is consistent with previous isotopic tracer experiments in which the coefficients and activation energies for $H_2{}^{18}O$, D_2O, and T_2O diffusion in ice were similar.

All the temperature-dependent isotopic tracer results for H_2O bulk diffusion in macroscopic crystalline ice from 238 to 270 K can be fairly accurately represented by an activation energy of $E_A = 14$ kcal/mol and a preexponential of $D_0 = 150$ cm^2/s. These kinetic parameters predict a bulk diffusion coefficient of $\sim 1 \times 10^{-17}$ cm^2/s at 160 K. In contrast, the measured HDO and $H_2{}^{18}O$ diffusion coefficient in the ultrathin ice multilayers on Ru(001) at 160 K was $D \sim 1.5 \times 10^{-15}$ cm^2/s or ∼150 times larger. This larger diffusion coefficient in the ultrathin ice films may provide information about molecular transport in the near surface region of molecular solids.

The proximity to a surface may perturb the adjacent bulk and affect various properties. One manifestation of this perturbation is the "quasi-liquid" layer on ice that is revealed by many experimental techniques.[1,34−40] Other theoretical simulations[41] and surface-sensitive probes[42] observed a very dynamic surface on the (0001) basal plane of hexagonal ice. The larger diffusion coefficients measured in the ultrathin ∼300 Å ice multilayers on Ru(001) may be another indication of a more "fluid-like" layer that enhances diffusion in the near surface region.

Very few experiments have investigated diffusion in the near surface region of molecular solids. Fortunately, there are nuclear magnetic resonance (NMR) studies of H_2O self-diffusion in the "quasi-liquid layer" on small ice particles from 253 to 273 K.[40] These NMR investigations indicate that the self-diffusion coefficient in the "quasi-liquid" layer is about 2 orders of magnitude larger than the self-diffusion coefficient in the single-crystal bulk. These NMR results are consistent with the ∼150 times larger diffusion coefficients measured in the ultrathin ice films on Ru(001). However, the activation energy for self-diffusion in the "quasi-liquid" layer was measured to be only $E_A = 5.6$ kcal/mol. This activation energy is very close to the activation energy for H_2O self-diffusion in liquid water of $E_A \sim 4.5$ kcal/mol.[2]

The diffusion coefficient in the ultrathin ice multilayers on Ru(001) may also be larger if the close proximity to the surface increases the number of interstitial defects and the H_2O diffusion occurs via an interstitial diffusion mechanism. In this case, the diffusion coefficient is given by $D = C_{int}D_{int}$ where D_{int} is the interstitial diffusion coefficient and C_{int} is the concentration of interstitials.[1] The number of interstitial defects may also be enhanced by the slight ∼4% lattice mismatch between the nearest-neighbor oxygen−oxygen distance in hexagonal ice[31] and the $(\sqrt{3} \times \sqrt{3})R30°$ lattice constant on Ru(001).[30]

The present HDO diffusion experiments were conducted at temperatures from $T = 153$ to 170 K. These ice film temperatures are significantly lower than the earlier isotopic tracer measurements[16−22] at $T = 238-273$ K near the ice melting point. The current experiments are also closer to the temperatures in the polar stratosphere from 180 to 210 K. The H_2O diffusion coefficients relevant to the polar stratosphere can be estimated using the temperature-dependent diffusion data from both the LITD and isotopic tracer[16−22] experiments.

The H_2O diffusion coefficients at stratospheric temperatures were calculated using an activation energy of $E_A = 17.0$ kcal/mol and preexponential of $D_0 = 4.2 \times 10^8$ cm^2/s from the LITD studies and an activation energy of $E_A = 14.0$ kcal/mol and preexponential of $D_0 = 150$ cm^2/s representative of the tracer measurements. Utilizing these diffusion kinetics, the H_2O diffusion coefficients varied from $D = 1.5 \times 10^{-15}-9.6 \times 10^{-13}$ cm^2/s at $T = 180$ K to $D = 4.0 \times 10^{-13}-8.6 \times 10^{-10}$ cm^2/s at $T = 210$ K. Consequently, H_2O molecules readily diffuse into

the crystalline ice bulk on the millisecond to microsecond time scale at stratospheric temperatures.

V. Conclusions

Laser-induced thermal desorption (LITD) techniques were used to study the diffusion of HDO into ultrathin single-crystal $H_2{}^{16}O$ ice multilayers grown epitaxially on Ru(001). The HDO diffusion coefficients were measured by LITD monitoring of the HDO coverage versus time during isothermal multilayer desorption. The concurrent isothermal desorption allows for depth-profiling of the H_2O-ice film. HDO was observed to diffuse readily into the underlying $H_2{}^{16}O$ multilayer. The diffusion coefficients for HDO varied from $D = (2.2 \pm 0.3) \times 10^{-16}$ to $D = (3.9 \pm 0.4) \times 10^{-14}$ cm^2/s for $T = 153-170$ K. Arrhenius analysis of the HDO diffusion data yielded a diffusion activation energy of $E_A = 17.0 \pm 1.0$ kcal/mol and a preexponential of $D_0 = (4.2 \pm 0.8) \times 10^8$ cm^2/s.

The activation energy measured for HDO diffusion is comparable to the activation energy of $E_A = 16.7 \pm 1.6$ kcal/mol obtained previously for $H_2{}^{18}O$ migration into crystalline hexagonal ice. The close agreement between the diffusion kinetics for HDO and $H_2{}^{18}O$ indicates that HDO transport in crystalline ice proceeds primarily via a molecular transport mechanism. The measured HDO diffusion coefficient at $T = 160$ K in the ultrathin single-crystal ice multilayers was $\sim$150 times larger than the predicted H_2O bulk diffusion constant at 160 K based on extrapolation using results from macroscopic ice samples at higher temperature. The larger diffusion coefficient may reflect the unique properties of ultrathin ice films with large surface-to-volume ratios. In particular, molecular transport in the ultrathin ice multilayer may be perturbed by close proximity to the ice surface.

Acknowledgment. This work was supported by the National Science Foundation under Grant CHE-9528473. G.C.W. gratefully acknowledges the National Science Foundation for an Atmospheric Training Grant (1995−1996). The authors also thank Professor R. Skodje for the generous use of a computer workstation to perform the diffusion modeling.

References and Notes

(1) For a comprehensive classic review of the chemical physics of ice, see: Hobbs, P. V. *Ice Physics*; Clarendon Press: Oxford, 1974.
(2) Eisenberg, D. W.; Kauzmann, W. *The Structure and Properties of Water*; Oxford University Press: New York, 1979.
(3) Nagle, J. F. In *Proton Transfer in Hydrogen-Bonded Systems*; Bountis, T., Ed.; Plenum Press: New York, 1992.
(4) Muto, H.; Matsura, K.; Nunome, K. *J. Phys. Chem.* **1992**, *96*, 5211.
(5) Molina, M. J.; Tso, T. L.; Molina, L. T.; Wang, F. C. Y. *Science* **1987**, *238*, 1253.
(6) Tolbert, M. A.; Rossi, M. J.; Malhorta, R.; Golden, D. M. *Science* **1987**, *238*, 1258.
(7) Solomon, S.; Garcia, R. R.; Rowland, F. S.; Wuebbles, D. J. *Nature* **1986**, *321*, 755.
(8) Turco, R. P.; Toon, O. B.; Hamill, P. *J. Geophys. Res.* **1989**, *94*, 16493.
(9) Hanson, D. R.; Ravishankara, A. R. *J. Geophys. Res.* **1991**, *96*, 5081.
(10) Onsager, L.; Runnels, L. K. *J. Chem. Phys.* **1969**, *50*, 1089.
(11) Bruni, F.; Consolini, G.; Careri, G. *J. Chem. Phys.* **1993**, *99*, 538.
(12) Consolini, G.; Bruni, F.; Careri, G. *J. Chem. Phys.* **1993**, *99*, 4227.
(13) Goto, K.; Hondoh, T.; Higashi, A. *Jpn. J. Appl. Phys.* **1986**, *25*, 351.
(14) Plummer, P. L. M. *J. Phys. (Paris)* **1987**, *48*, 45.
(15) Hondoh, T.; Goto, A.; Hoshi, R.; Ono, T.; Anzai, H.; Kawase, R.; Pimienta, P.; Mae, S. *Rev. Sci. Instrum.* **1989**, *60*, 2494.
(16) Dengel, O.; Riehl, N. *Phys. Condens. Mater.* **1963**, *1*, 191.
(17) Kuhn, W.; Thurkauf, M. *Helv. Chim. Acta* **1958**, *41*, 938.
(18) Itagaki, J. *J. Phys. Soc. Jpn.* **1964**, *19*, 1081.
(19) Itagaki, J. *J. Phys. Soc. Jpn.* **1967**, *22*, 427.
(20) Blicks, H.; Dengel, O.; Riehl, N. *Phys. Condens. Mater.* **1966**, *4*, 375.
(21) Delibaltas, P.; Dengel, O.; Helmreich, D.; Riehl, N.; Simon, H. *Phys. Condens. Mater.* **1966**, *5*, 166.
(22) Ramseier, R. O. *J. Appl. Phys.* **1967**, *38*, 2553.
(23) Brown, D. E.; George, S. M. *J. Phys. Chem.* **1996**, *100*, 15460.
(24) Mak, C. H.; Brand, J. L.; Deckert, A. A.; George, S. M. *J. Chem. Phys.* **1986**, *85*, 1676.
(25) Brown, D. E.; George, S. M.; Huang, C.; Wong, E. K. L.; Rider, K. B.; Smith, R. S.; Kay, B. D. *J. Phys. Chem.* **1996**, *100*, 4988.
(26) Deckert, A. A.; Brand, J. L.; Arena, M. V.; George, S. M. *Surf. Sci.* **1989**, *208*, 441.
(27) George, S. M.; DeSantolo, A. M.; Hall, R. B. *Surf. Sci.* **1985**, *159*, L425.
(28) Pruppacher, H. R.; Klett, J. D. *Microphysics of Clouds and Precipitation*; D. Reidel Publishing: Dordrecht, Holland, 1980.
(29) Toon, O. B.; Turco, R. P.; Jordan, J.; Goodman, J.; Ferry, G. *J. Geophys. Res.* **1989**, *94*, 11359.
(30) *Americal Institute of Physics Handbook*, 3rd ed.; McGraw-Hill: New York, 1982.
(31) LaPlaca, S.; Post, B. *Acta Crystallogr.* **1960**, *13*, 503.
(32) Haynes, D. R.; Tro, N. J.; George, S. M. *J. Phys. Chem.* **1992**, *96*, 8502.
(33) Crank, J. *The Mathematics of Diffusion*; Clarendon Press: Oxford, 1975.
(34) Beaglehole, D.; Nason, D. *Surf. Sci.* **1980**, *96*, 357.
(35) Gilpin, R. R. *J. Colloid Interface Sci.* **1980**, *77*, 435.
(36) Nason, D.; Fletcher, N. H. *J. Chem. Phys.* **1975**, *62*, 4444.
(37) Elbaum, M.; Lipson, S. G.; Dash, J. G. *J. Cryst. Growth* **1993**, *129*, 491.
(38) Golecki, I.; Jaccard, C. *J. Phys. C: Solid State Phys.* **1978**, *11*, 4229.
(39) Furukawa, Y.; Yamamoto, M.; Kuroda, T. *J. Cryst. Growth* **1987**, *82*, 665.
(40) Mizuno, Y.; Hanafusa, N. *J. Phys. C1* **1987**, *48*, 511.
(41) Kroes, G.-J. *Surf. Sci.* **1992**, *275*, 365.
(42) Materer, N.; Starke, U.; Barbieri, A.; Van Hove, M. A.; Somorjai, G. A.; Kroes, G.-J.; Minot, C. *J. Phys. Chem.* **1995**, *99*, 6267.